

# Mobility anisotropy in monolayer black phosphorus due to scattering by charged impurities

Yue Liu, Tony Low,<sup>\*</sup> and P. Paul Ruden*Department of Electrical and Computer Engineering, University of Minnesota, Minneapolis, Minnesota 55455, USA*

(Received 22 December 2015; published 1 April 2016)

We explore the charged-impurity-scattering-limited mobility of electrons and holes in monolayer black phosphorus (BP), a highly anisotropic material. Taking full account of the anisotropic electronic structure in effective mass approximation, the zero-temperature momentum relaxation time and the charge carrier mobility are calculated based on the Boltzmann transport equation. For carrier densities accessible in experiments, we obtain anisotropy ratios of 3–4. These results are somewhat larger than mobility anisotropy ratios determined experimentally for multilayer BP samples, but due to the complex dependence of the scattering rates on the anisotropy, they are strikingly smaller than the effective mass ratios.

DOI: [10.1103/PhysRevB.93.165402](https://doi.org/10.1103/PhysRevB.93.165402)

## I. INTRODUCTION

Black phosphorus (BP), its puckered layered form, is one of the thermodynamically more stable phases of phosphorus at ambient temperature and pressure [1–4]. The recent successful exfoliation of BP [5–6] multilayers and monolayers has triggered much interest in this material. Multilayer BP has a direct bandgap that spans the range of 0.3–1.5 eV, depending on the number of layers [7–10], thus making it an excellent candidate material for infrared optoelectronics [11–13]. Its good electrical transport properties, with the highest carrier mobility after graphene, and a finite electronic gap larger than  $k_B T$  at room temperature, also make it a promising candidate for nanoelectronics [15,16]. Since each BP layer has a puckered structure due to  $sp^3$  hybridization, the material has highly anisotropic electrical and optical properties. This includes anisotropic charge carrier mobility [4,5,14,17] and linear dichroism in optical absorption [2,8–10,14,18]. Indeed, the BP crystal structure gives rise to highly anisotropic energy bands with the in-plane effective masses along the two crystal axes, armchair and zigzag, differing by an order of magnitude. For example, the effective masses in bulk BP were measured with cyclotron resonance techniques to be  $m_{xx}^e = m_{xx}^h = 0.08m_0$  and  $m_{yy}^e = 0.7m_0$ ,  $m_{yy}^h = 1.0m_0$  [19]. For monolayer BP, these masses were predicted to be  $m_{xx}^e = m_{xx}^h = 0.15m_0$ , with  $m_{yy}^e$  and  $m_{yy}^h$  being the same as in bulk BP [8,20]. A very naïve expectation, therefore, based on a constant momentum relaxation time, is that the charge carrier mobility anisotropy ratios might be roughly between 4.5 and 12. However, low temperature transport measurements on multilayer BP thus far have yielded anisotropy ratios of between 1.5 to 2 [6,14,17]. Reconciling the large anisotropy in its electronic bands with the moderate mobility anisotropy observed is important for the fundamental understanding of transport properties in BP.

There have been several theoretical studies on the anisotropic transport properties of BP [9,21,22]; however, the anisotropy of scattering was not treated explicitly. This is because the momentum relaxation time evaluated with the Boltzmann transport equation does not have a closed form solution for an anisotropic material [23–26]. The problem has been avoided so far with approximations that are not entirely

suitable. In this paper, we describe our methodology of solving for the charged-impurity-scattering-limited anisotropic mobility of BP with the Boltzmann transport equation in relaxation time approximation, accounting for the full anisotropy of the problem. The momentum relaxation time depends not only on the wave vector of the incoming state, but also on the direction of electric field. We found that the mobility anisotropy ratio is highly sensitive to the distribution of the charged impurities and can range from 1.5 to 7. For uniformly distributed impurities in the substrate, we estimated mobility anisotropy ratios of about  $\sim 3.5$ –4 for monolayer BP, i.e. significantly less than the effective mass anisotropy ratio. We discuss how mobility and its anisotropy depend on impurity distance and charge carrier density.

## II. MODEL DESCRIPTION

We consider monolayer BP on an insulating substrate with charged impurities located in the substrate at a distance that is generally large compared to the thickness of the BP layer, as illustrated in Fig. 1(a). The anisotropic energy dispersion of BP in the vicinity of the conduction band minimum at the  $\Gamma$  point is described in effective mass approximation as [1,2]

$$E(\vec{k}) = \frac{\hbar^2}{2} \left( \frac{1}{m_{xx}} k_x^2 + \frac{1}{m_{yy}} k_y^2 \right), \quad (1)$$

where  $m_{xx}$  and  $m_{yy}$  are the effective masses along  $x$  (armchair) and  $y$  (zigzag) directions. Charge carriers in this conduction band interact with the charged impurities in the substrate via the Coulomb interaction. Coulomb scattering is an elastic process, and Fig. 1(b) illustrates the scattering phase space from the incoming state  $|\vec{k}_i\rangle$  to the outgoing state  $|\vec{k}_j\rangle$ . The transition rate  $P_{\vec{k}_i, \vec{k}_j}^*$  can be expressed by Fermi's golden rule

$$P_{\vec{k}_i, \vec{k}_j}^* = \frac{2\pi}{\hbar} |\langle \vec{k}_j | H | \vec{k}_i \rangle|^2 n_{\text{imp}} \delta[E(\vec{k}_i) - E(\vec{k}_j)]. \quad (2)$$

Here,  $H$  is the Hamiltonian describing the screened Coulomb interaction between the charge carriers and charged impurities of sheet density  $n_{\text{imp}}$ . (In this paper, we assume a typical impurity concentration of  $n_{\text{imp}} = 10^{12} \text{ cm}^{-2}$  unless stated otherwise.) The constant density of states (DOS)  $g_{2D} = \frac{m_d}{\pi \hbar^2}$ , where the DOS effective mass  $m_d = \sqrt{m_{xx} m_{yy}}$  leads to a simple expression for the linear, static polarization function  $\Pi(\vec{q})$ . Taking the image charge into account, the matrix

<sup>\*</sup>tlow@umn.edu

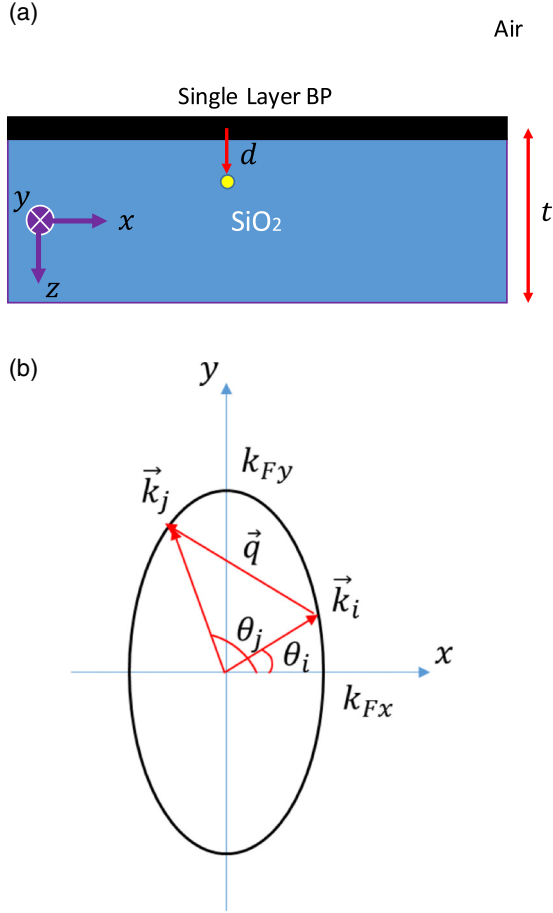


FIG. 1. Model structure schematic. (a) BP/SiO<sub>2</sub> as semiconductor/insulator layer structure, with a charged impurity represented by a yellow dot at distance  $d$ . (b) Charged impurity scattering occurs on an ellipsoidal phase space contour, with  $x$  and  $y$  being the armchair and zigzag directions of BP, respectively.

element in Eq. (2) is written as [27]

$$|\langle \vec{k}_j | H | \vec{k}_i \rangle| = \frac{2\pi e^2 e^{-q \cdot d}}{q\kappa + 2\pi e^2 \Pi(\vec{q})}. \quad (3)$$

Since our focus is on elastic scattering, we use a static effective dielectric constant of  $\kappa = \frac{\kappa_{\text{air}} + \kappa_{\text{SiO}_2}}{2} \approx 2.5$  for the air/SiO<sub>2</sub> (substrate) half spaces. Here,  $d$  is the out-of-plane vertical distance between the impurity and BP layer. The scattering wave vector is denoted by  $\vec{q} = \vec{k}_j - \vec{k}_i$ , and  $\Pi(\vec{q})$  is the anisotropic two-dimensional (2D) polarizability of BP. In general,  $\Pi(\vec{q})$  depends on  $\vec{q}$  and, in the limit of zero temperature, reduces to [28–30]

$$\Pi(\vec{q}) = g_{2D} \text{Re} \left[ 1 - \sqrt{1 - \frac{4E_F}{E(\vec{q})}} \right], \quad (4)$$

where  $E_F = \frac{\hbar^2 \pi n}{m_d}$  is Fermi energy, and  $n$  is the electron (or hole) density. Furthermore, it can be shown that  $\Pi(\vec{q})$  is isotropic for  $q \equiv |\vec{q}|$  constrained by  $q \leq 2|\vec{k}_F \cdot \hat{q}|$ , which corresponds to the phase space illustrated in Fig. 1(b). Thus,  $\Pi(\vec{q})$  simply reduces to  $g_{2D}$  in the zero-temperature limit [30].

For finite temperature, scattering is still elastic but no longer limited to the Fermi surface. Therefore, an anisotropic  $\Pi(\vec{q})$  in Eq. (4) is needed.

We are now ready to write down the anisotropic momentum relaxation time  $\tau_m$ , derived from the Boltzmann transport equation (see Supplemental Material [31])

$$\frac{1}{\tau_m(\hat{\xi}, \vec{k}_i)} = \frac{1}{(2\pi)^2} \int_{\text{all } \vec{k}_j} d^2 \vec{k}_j P_{\vec{k}_i, \vec{k}_j} \left\{ 1 - \frac{[\hat{\xi} \cdot \vec{v}(\vec{k}_j)] \tau_m(\hat{\xi}, \vec{k}_j)}{[\hat{\xi} \cdot \vec{v}(\vec{k}_i)] \tau_m(\hat{\xi}, \vec{k}_i)} \right\}. \quad (5)$$

Here,  $\hat{\xi}$  is the direction of the applied electric field and  $\vec{v}(\vec{k}) = \frac{1}{\hbar} \nabla_{\vec{k}} E(\vec{k})$  is the group velocity. For  $T = 0$  K, scattering only occurs at the Fermi level, that is  $E(\vec{k}_i) = E_F$  in Eq. (2). It is worth pointing out that the relaxation time of an anisotropic material depends both on the direction of the electric field  $\hat{\xi}$  and on the wave vector of incoming state  $|\vec{k}_i\rangle$ . The magnitude of the electric field  $|\hat{\xi}|$  is of course irrelevant in linear response.

For an isotropic 2D electron gas,  $m_{xx} = m_{yy}$ , and the relaxation time is the same for all  $|\vec{k}_i\rangle$  and does not depend on  $\hat{\xi}$ , i.e.  $\tau_m(\hat{\xi}, \vec{k}_i) = \tau_{\text{iso}}$ . Then Eq. (5) can be reduced to an explicit integral

$$\frac{1}{\tau_{\text{iso}}} = \frac{1}{(2\pi)^2} \int_{\text{all } \vec{k}_j} d^2 \vec{k}_j P_{\vec{k}_i, \vec{k}_j} (1 - \cos \theta_{ij}), \quad (6)$$

where  $\theta_{ij}$  is the scattering angle between  $|\vec{k}_i\rangle$  and  $|\vec{k}_j\rangle$ .

The strongly anisotropic electronic structure of BP ( $\frac{m_{yy}}{m_{xx}} \approx 7$ ) requires solving for the momentum relaxation time  $\tau_m(\hat{\xi}, \vec{k}_i)$  from the implicit integral in Eq. (5). We discuss briefly our numerical procedure. First, we recast Eq. (5) in cylindrical coordinates, arriving at

$$\frac{1}{\tau_m(\hat{\xi}, \vec{k}_i)} = \frac{1}{(2\pi)^2} \int_0^{2\pi} d\theta_j \left\{ \beta M_{i,j} \frac{1}{2\beta} \times \left[ 1 - \frac{\alpha[\vec{k}_j = (\beta, \theta_j)] \tau_m[\hat{\xi}, \vec{k}_j = (\beta, \theta_j)]}{\alpha(\vec{k}_i) \tau_m(\hat{\xi}, \vec{k}_i)} \right] \right\}, \quad (7)$$

where

$$M_{i,j} = \frac{2\pi}{\hbar} |\langle \vec{k}_j | H | \vec{k}_i \rangle|^2 n_{\text{imp}} \left( \frac{\hbar^2 \cos^2 \theta_j}{2m_{xx}} + \frac{\hbar^2 \sin^2 \theta_j}{2m_{yy}} \right)^{-1}, \quad (8)$$

and we introduce  $\beta = k_j \sqrt{\frac{E(\vec{k}_j)}{E(\vec{k}_i)}}$ ,  $\alpha(\vec{k}) = \hat{\xi} \cdot \vec{v}(\vec{k})$  to simplify the notation. We further identify  $W(\theta_j) = \left( \frac{\hbar^2 \cos^2 \theta_j}{2m_{xx}} + \frac{\hbar^2 \sin^2 \theta_j}{2m_{yy}} \right)^{-1}$ , which can be viewed as a DOS along the energy contour. In arriving at Eq. (7), we made use of the  $\delta$  function property,  $\delta(\beta^2 - k_j^2) = \frac{1}{2\beta_j} [\delta(k_j + \beta) + \delta(k_j - \beta)]$ . We rewrite Eq. (7) as a system of linear equations for  $\tau_i \equiv \tau_m(\hat{\xi}, \vec{k}_i)$ , where  $i = 1, \dots, N$  stands for the  $i$ th discrete incoming state  $|\vec{k}_i\rangle$  along the elliptical  $k$  contour. Writing  $b = \frac{1}{(2\pi)^2} \frac{\Delta \theta_j}{2}$ , with

$\Delta\theta_j = \frac{2\pi}{N-1}$ , and  $\alpha_i \equiv \alpha(\vec{k}_i)$ , Eq. (7) can be recast as

$$\begin{aligned}
 & -\alpha_i + b \sum_j M_{i,j} \alpha_j \tau_i \\
 & = b(M_{i,1}\alpha_1 M_{i,2}\alpha_2 \cdots M_{i,N}\alpha_N) \begin{pmatrix} \tau_1 \\ \tau_2 \\ \vdots \\ \tau_N \end{pmatrix}, \quad (9)
 \end{aligned}$$

for all  $i$ . Equation (9) can be written in matrix form as  $[T]|\tau_m\rangle = |\alpha\rangle$ , and the array of  $\tau_m$  is found by inverting  $[T]$  iteratively. In our computation, we employ a total of  $N = 1000$  points to achieve convergence of  $\frac{\text{norm}(|\tau_m\rangle' - |\tau_m\rangle)}{\text{norm}(|\tau_m\rangle)} < 0.01$ , with  $\text{norm}(|\tau_m\rangle) = \sqrt{\tau_1^2 + \tau_2^2 + \cdots + \tau_N^2}$ . Here,  $|\tau_m\rangle'$  represents the  $(l+1)$ th iteration. To the best of our knowledge, no similar method for solving for the relaxation time in anisotropic media has been presented. However, it is noteworthy to mention that nonclosed-form solutions of the Boltzmann transport equation are also encountered when dealing with isotropic materials and inelastic processes [23,24].

### III. ANISOTROPIC MOMENTUM RELAXATION TIME

Following the model described in the last section, we compute the anisotropic momentum relaxation times  $\tau_m(\hat{x}, \vec{k}_i)$  and  $\tau_m(\hat{y}, \vec{k}_i)$ , assuming  $T = 0$  K, and hole effective masses of  $m_{xx} = 0.15m_0$  and  $m_{yy} = 1.0m_0$ , unless otherwise stated [8]. The results are plotted in Fig. 2(a). The average momentum relaxation times  $\langle\tau_m\rangle = \frac{1}{N} \sum_i \tau_m(\hat{\xi}, \vec{k}_i)$  are plotted in Fig. 2(b). The calculated momentum relaxation time is on the order of picoseconds for the assumed impurity concentration, with  $\tau_m(\hat{y}, \vec{k}_i) > \tau_m(\hat{x}, \vec{k}_i)$ , and a relaxation time anisotropy ratio of  $\approx 5$  is obtained. Momentum relaxation favors backscattering against the direction of the electric field. This is apparent from the  $1 - \frac{[\hat{\xi} \cdot \vec{v}(\vec{k}_j)]\tau_m(\hat{\xi}, \vec{k}_j)}{[\hat{\xi} \cdot \vec{v}(\vec{k}_i)]\tau_m(\hat{\xi}, \vec{k}_i)}$  term in Eq. (5), which in the isotropic case will reduce to  $1 - \cos\theta_j$  in Eq. (6). Due to the band anisotropy, backscattering requires a larger  $q$  when  $\hat{\xi}$  is along  $y$ . Since  $M_{i,j}$  decreases with increasing  $q$ , this leads to a larger momentum relaxation time, i.e.  $\tau_m(\hat{y}, \vec{k}_i) > \tau_m(\hat{x}, \vec{k}_i)$ .

In addition to its dependence on the direction of electric field,  $\tau_m$  also depends on the incoming state wave vector  $\vec{k}_i$ . Considering for simplicity the case of  $d = 0$ , the scattering matrix element  $M_{i,j}$  is independent of the initial state  $\vec{k}_i$ , if  $q \ll \frac{2\pi e^2}{\kappa} g_{2D}$ . Since  $q$  increases with the Fermi energy, one can identify a carrier density at which  $\tau_m$  changes from being independent of  $\vec{k}_i$  to being  $\vec{k}_i$  dependent. Figure 2(a) reflects this behavior. When the carrier density is small enough, such that  $q$  is negligible compared to the screening term  $\frac{2\pi e^2}{\kappa} g_{2D}$ ,  $\tau_m$  is independent of  $\vec{k}_i$  [red curves in Fig. 2(a)], whereas for large  $n$ , we observe that  $\tau_m$  has minima when  $\theta_i = \frac{\pi}{2}$  and  $\frac{3\pi}{2}$ . The scattering matrix element  $M_{i,j}$  in Eq. (8) depends on an effective angular DOS  $W(\theta_j)$ . In the limit of extreme anisotropy, i.e.  $m_{yy} \gg m_{xx}$ , the maxima of  $W(\theta_j)$  occur near  $\theta_j = \frac{\pi}{2}$  and  $\frac{3\pi}{2}$ . It can be seen from Fig. 1(b) that  $q$  is zero in that limit when  $\theta_i = \frac{\pi}{2}$ , and  $M_{i,j}$  reaches a maximum. As a result,  $\tau_m$  has a minimum at  $\theta_i = \frac{\pi}{2}$  for high carrier densities. Increasing carrier density  $n$  increases the effective  $q$  involved

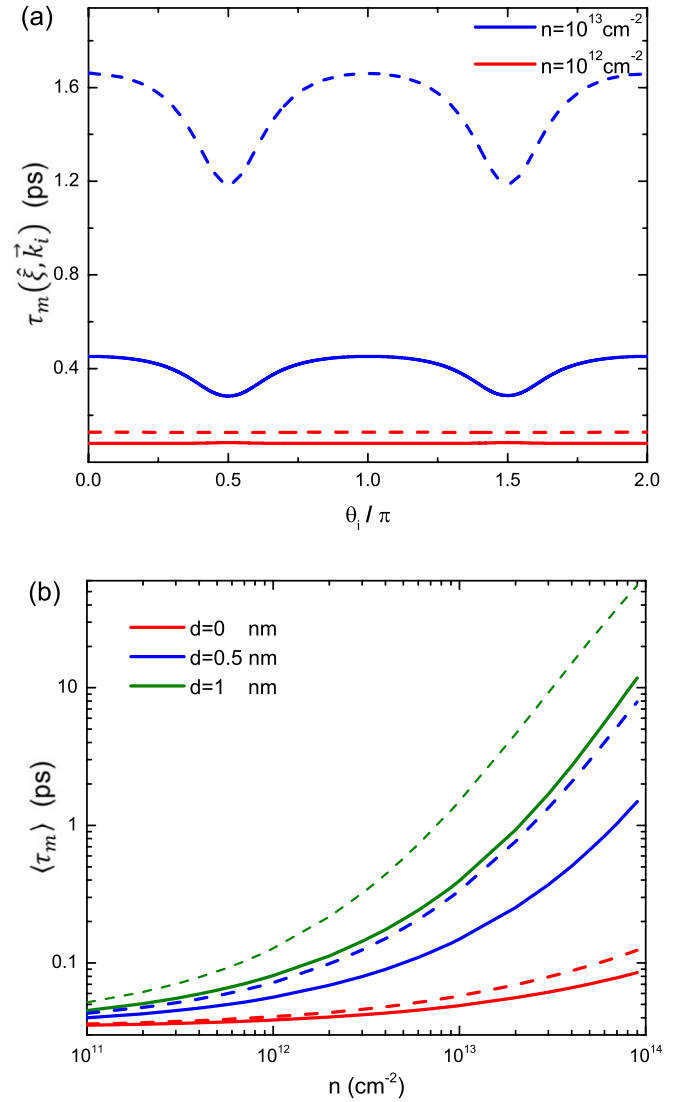


FIG. 2. Calculated momentum relaxation time  $\tau_m$  and its dependence on impurity distance  $d$ , carrier density  $n$ , and electric field direction  $\hat{\xi}$ . Solid and dashed lines are for  $\hat{\xi}$  along  $x$  and  $y$  directions, respectively. (a)  $\tau_m$  varies with the initial wave vector  $\vec{k}_i$  for  $d = 1$  nm,  $\tau_m(\hat{x}, \vec{k}_i) < \tau_m(\hat{y}, \vec{k}_i)$ . (b) Average  $\langle\tau_m\rangle$  dependence on  $n$ , for different  $d$ .

in scattering. Therefore, increasing  $d$  and/or  $n$  lead to smaller  $M_{i,j}$  and larger  $\langle\tau_m\rangle$ , as shown in Fig. 2(b).

### IV. ANISOTROPIC MOBILITY

With  $\tau_m(\hat{\xi}, \vec{k}_i)$  computed, the effective mobility  $\mu$  or conductivity  $\sigma$  at  $T = 0$  K can be investigated. For  $\hat{\xi}$  along the  $x$  direction, we define the relevant mobility as

$$\mu_{xx} = \frac{g_s e}{(2\pi)^2 n} \int d^2 \vec{k} v_x^2(\vec{k}) \tau_m(\hat{x}, \vec{k}) \frac{\partial f}{\partial E}. \quad (10)$$

An analogous mobility can be defined for  $\hat{\xi}$  along the  $y$  direction. Here,  $\mu_{xx}$  and  $\mu_{yy}$  are nonzero elements of the mobility tensor  $v_x(\vec{k}) = \frac{\hbar k_x}{m_{xx}}$ ,  $g_s = 2$  is the spin degeneracy,  $\frac{\partial f}{\partial E} = \frac{1}{k_B T} f(E)[1 - f(E)]$  is a  $\delta$  function at zero temperature

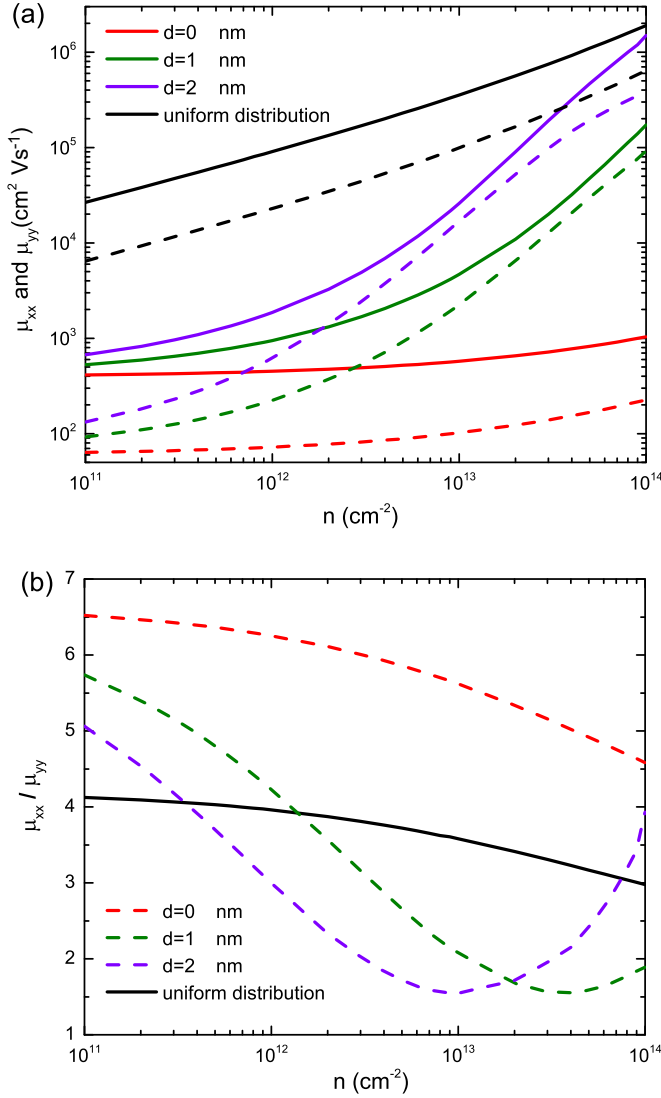


FIG. 3. Calculated mobility and anisotropy ratio, related to impurity distance  $d$ , and carrier density  $n$ . Impurity density  $n_{\text{imp}} = 10^{12} \text{ cm}^{-2}$  (a) mobility  $\mu_{xx} > \mu_{yy}$ . Solid and dashed lines represent  $\mu_{xx}$  and  $\mu_{yy}$ , respectively. (b) Anisotropy ratio  $\frac{\mu_{xx}}{\mu_{yy}}$  changing as a function of  $n$ . Solid and dashed lines represent uniform model and constant distance model, respectively.

[ $f(E)$  is the Fermi-Dirac distribution]. As  $d$  or  $n$  increases,  $\tau_m$  increases as previously discussed, leading to increasing mobility, as shown in Fig. 3(a). Although  $\tau_m(\hat{x}, \vec{k}_i) < \tau_m(\hat{y}, \vec{k}_i)$ , we find  $\mu_{xx} > \mu_{yy}$ . The mobility depends on  $(\hat{\xi} \cdot \vec{v})^2$ ; hence, the mobility anisotropy ratio is  $\frac{\mu_{xx}}{\mu_{yy}} \sim \left(\frac{m_{yy}}{m_{xx}}\right)^2 \frac{\langle \tau_m(\hat{x}, \vec{k}_i) \rangle}{\langle \tau_m(\hat{y}, \vec{k}_i) \rangle}$ . In this case,  $\left(\frac{m_{yy}}{m_{xx}}\right)^2$  is approximately equal to 44. The smaller anisotropy ratio observed is due to the opposing trend of the momentum relaxation time. As illustrated by dashed lines in Fig. 3(b), only when  $d = 0$  does the anisotropy ratio decrease monotonically as a function of  $n$  in the range investigated. When  $d \neq 0$ , for each dashed  $\frac{\mu_{xx}}{\mu_{yy}}$  curve, there is a minimum located around  $n_{\text{cut}} = (2\pi d^2)^{-1}$  that originates from the scattering matrix element  $M_{i,j}$ , depending exponentially on  $q \cdot d$ . Therefore,  $d$  defines an effective cutoff for  $q$ , and correspondingly a

finite  $n_{\text{cut}}$ . Besides, all curves approximately share a similar minimum of  $\approx 1.5$ . For larger  $d$ , the minimum at  $\sim (2\pi d^2)^{-1}$  is found at smaller  $n$ . It is interesting to note that our calculated anisotropy ratio varies from 1.5 to 7 depending on the values of  $n$  and  $d$ .

To eliminate the effect of the impurity distance  $d$ , we employ a uniform impurity distribution model. Using  $n_0 = \frac{n_{\text{imp}}}{t}$  to replace  $n_{\text{imp}}$  in Eq. (2), where  $t = 300 \text{ nm}$  is the total thickness of the  $\text{SiO}_2$  layer, we replace the matrix element in Eq. (3) with  $|\langle \vec{k}_j | H | \vec{k}_i \rangle| = \frac{2\pi e^2 e^{-qz}}{q\kappa + 2\pi e^2 \Pi(q)}$ . The mobility and anisotropy ratios calculated using the uniform impurity distribution model are shown as black curves in Figs. 3(a) and 3(b). As we stated above, increasing distance leads to increasing mobility. The curve varies similarly to the  $d = 0$  case and is now also monotonic as a function of  $n$ , which can be understood as the impurities nearest to BP have the largest influence. Uniform distribution of the impurities also reduces the sensitivity to  $n$ .

## V. COMPARISON WITH EXPERIMENTS

In our calculation for monolayer BP, we find hole mobilities on the order of  $10^3$ – $10^4 \text{ cm}^2 \text{ Vs}^{-1}$  for carrier densities  $10^{12}$ – $10^{13} \text{ cm}^{-2}$  and transport along the low effective mass direction. On the experimental side, hole Hall mobility of order  $10^3 \text{ cm}^2 \text{ Vs}^{-1}$  at carrier density of about  $6.7 \times 10^{12} \text{ cm}^{-2}$  has been observed at low temperature [14,17]. This would suggest that our assumed impurity concentration of  $n_{\text{imp}} = 10^{12} \text{ cm}^{-2}$  probably underestimates the experimental situation, or there could be other sources of scattering, e.g. neutral impurities, short-range trap states, and surface roughness. A better quantity for comparison with experiment may be the anisotropy ratio  $\frac{\mu_{xx}}{\mu_{yy}}$ , which does not depend on  $n_{\text{imp}}$ .

The mobility anisotropy ratios for holes are evaluated to be  $\sim 3.5$ – $4$ , across the range of hole densities shown in Fig. 3(b). Using  $m_{xx}^e = 0.15m_0$  and  $m_{yy}^e = 0.7m_0$ , we calculate the electron mobility anisotropy ratio as  $\sim 2.4$ – $3.2$  across the same range of carrier densities. These anisotropy ratios are larger than  $\frac{\mu_{xx}}{\mu_{yy}} \approx 1.8$  obtained from Hall hole mobility measurements at 120 K [14], and results obtained from nonlocal resistance measurements, which yielded  $\frac{\mu_{xx}}{\mu_{yy}} \approx 1.66 \pm 1.1$  at 5–50 K. On the other hand, angle-resolved field effect mobility measurements yield a ratio of  $\sim 2$ – $4$  [17]. If we base our calculation on the effective masses of bulk BP [19], the resulting anisotropy ratio is larger and deviates further from experiment.

One may identify several possible reasons for the discrepancy. First, few-layer BP samples with a thickness around 10 nm were used in the experiments. Their multisubband electronic structures can lead to scattering between subbands. Furthermore, the effective masses in few-layer samples are at present uncertain. Indeed, first-principle calculations yield a wide range of effective masses depending on the method used [9,32–34]. However, our transport calculation would suggest that the mass anisotropy ratio in these experimental samples should be less than 10, based on the measured mobility anisotropy. Additionally, experimental measurements were performed at 10–120 K, where electron-phonon scattering is not completely quenched, and might reduce the anisotropy.

The mobility anisotropy observed in experiments so far is relatively insensitive to carrier concentration and more consistent with our case of uniform impurity distribution. This might suggest that charged impurities in experimental samples are probably due to bulk dopants, perhaps introduced as grown. With advances in BP growth techniques, one may eventually approach situations where the mobility is limited by interfacial impurities like in the case of state-of-the-art semiconductor devices. We defer the study of these issues to future work. We also executed a calculation of the mobility assuming an extremely short-range potential, i.e. by replacing Eq. (3) with a  $q$ -independent potential, and found a mobility anisotropy ratio of  $\sim 4.67$ , independent of  $n$ .

To summarize, we have calculated the charged-impurity-scattering-limited hole mobility of monolayer BP within a Boltzmann transport model, considering the full anisotropy of the transport and electronic structure explicitly. We explored the momentum relaxation time dependence on the electric field direction as well as on the incoming wave vector. Although  $\tau_m(\hat{x}, \vec{k}_i) < \tau_m(\hat{y}, \vec{k}_i)$ , we find  $\mu_{xx} > \mu_{yy}$  with anisotropy mobility ratios  $\sim 3.5$ – $4$ . The influence of the effective mass ratio is compensated by the opposing trend of the relaxation time. The approach outlined in this paper can also be applied to other emerging anisotropic 2D materials, such as the 1T phase of transition metal dichalcogenides [35–37] and transition metal trichalcogenides [38–40].

- 
- [1] R. W. Keyes, *Phys. Rev.* **92**, 580 (1953).
- [2] A. Morita, *Appl. Phys. A* **39**, 227 (1986).
- [3] R. J. Wu, M. Topsakal, T. Low, M. C. Robbins, N. Haratipour, J. S. Jeong, R. M. Wentzcovitch, S. J. Koester, and K. A. Mkhoyan, *J. Vac. Sci. Technol., A* **33**, 060604 (2015).
- [4] H. Liu, Y. Du, Y. Deng, and P. D. Ye, *Chem. Soc. Rev.* **44**, 2732 (2015).
- [5] L. Li, Y. Yu, G. J. Ye, Q. Ge, X. Ou, H. Wu, D. Feng, X. H. Chen, and Y. Zhang, *Nat. Nanotechnol.* **9**, 372 (2014).
- [6] H. Liu, A. T. Neal, Z. Zhu, D. Tomanek, and P. D. Ye, *ACS Nano* **8**, 4033 (2014).
- [7] A. Castellanos-Gomez, L. Vicarelli, E. Prada, J. O. Island, K. L. Narasimha-Acharya, S. I. Blanter, D. J. Groenendijk, M. Buscema, G. A. Steele, J. V. Alvarez, H. W. Zandbergen, J. J. Palacios, and H. S. J. van der Zant, *2D Mater.* **1**, 025001 (2014).
- [8] T. Low, A. S. Rodin, A. Carvalho, Y. Jiang, H. Wang, F. Xia, and A. H. Castro Neto, *Phys. Rev. B* **90**, 075434 (2014).
- [9] J. Qiao, X. Kong, Z.-X. Hu, F. Yang, and W. Ji, *Nat. Commun.* **5**, 4475 (2014).
- [10] V. Tran, R. Soklaski, Y. Liang, and L. Yang, *Phys. Rev. B* **89**, 235319 (2014).
- [11] M. Engel, M. Steiner, and P. Avouris, *Nano Lett.* **14**, 6414 (2014).
- [12] N. Youngblood, C. Chen, S. J. Koester, and M. Li, *Nat. Photon.* **9**, 247 (2015).
- [13] T. Low, M. Engel, M. Steiner, and P. Avouris, *Phys. Rev. B* **90**, 081408 (2014).
- [14] F. Xia, H. Wang, and Y. Jia, *Nat. Commun.* **5**, 4458 (2014).
- [15] Y. Du, H. Liu, Y. Deng, and P. D. Ye, *ACS Nano* **8**, 10035 (2014).
- [16] N. Haratipour, M. C. Robbins, and S. J. Koester, *IEEE Electron Device Lett.* **36**, 411 (2015).
- [17] A. Mishchenko, Y. Cao, G. L. Yu, C. R. Woods, R. V. Gorbachev, K. S. Novoselov, A. K. Geim, and L. S. Levitov, *Nano Lett.* **15**, 6991 (2015).
- [18] H. Yuan, X. Liu, F. Afshinmanesh, W. Li, G. Xu, J. Sun, B. Lian, A. G. Curto, G. Ye, Y. Hikita, Z. Shen, S.-C. Zhang, X. Chen, M. Brongersma, H. Y. Hwang, and Y. Cui, *Nat. Nanotechnol.* **10**, 707 (2015).
- [19] S.-i. Narita, S.-i. Terada, S. Mori, K. Muro, Y. Akahama, and S. Endo, *J. Phys. Soc. Jpn.* **52**, 3544 (1983).
- [20] A. S. Rodin, A. Carvalho, and A. H. Castro Neto, *Phys. Rev. Lett.* **112**, 176801 (2014).
- [21] Z.-Y. Ong, G. Zhang, and Y. W. Zhang, *J. Appl. Phys.* **116**, 214505 (2014).
- [22] B. Liao, J. Zhou, B. Qiu, M. S. Dresselhaus, and G. Chen, *Phys. Rev. B* **91**, 235419 (2015).
- [23] D. L. Rode, *Phys. Rev. B* **3**, 3287 (1971). See also the comprehensive review: D. L. Rode, R. K. Willardson, and A. C. Beer, *Transp. Phenom.* **10**, 1 (1975).
- [24] J. R. Meyer and F. J. Bartoli, *Phys. Rev. B* **24**, 2089 (1981).
- [25] M. V. Fischetti, *J. Appl. Phys.* **89**, 1232 (2001).
- [26] M. V. Fischetti, Z. Ren, P. M. Solomon, M. Yang, and K. Rim, *J. Appl. Phys.* **94**, 1079 (2003).
- [27] T. Ando, A. B. Fowler, and F. Stern, *Rev. Mod. Phys.* **54**, 437 (1982).
- [28] F. Stern, *Phys. Rev. Lett.* **18**, 546 (1967).
- [29] D. A. Dahl and L. J. Sham, *Phys. Rev. B* **16**, 651 (1977).
- [30] T. Low, R. Roldan, H. Wang, F. Xia, P. Avouris, L. M. Moreno, and F. Guinea, *Phys. Rev. Lett.* **113**, 106802 (2014).
- [31] See Supplemental Material at <http://link.aps.org/supplemental/10.1103/PhysRevB.93.165402> for the derivation of Eq. (5) from the Boltzmann transport equation.
- [32] X. Han, H. M. Stewart, S. A. Shevlin, C. R. A. Catlow, and Zheng Xiao Guo, *Nano Lett.* **14**, 4607 (2014).
- [33] M. Elahi, K. Khaliji, S. M. Tabatabaei, M. Pourfath, and R. Asgari, *Phys. Rev. B* **91**, 115412 (2015).
- [34] S. Yuan, A. N. Rudenko, and M. I. Katsnelson, *Phys. Rev. B* **91**, 115436 (2015).
- [35] S. Tongay, H. Sahin, C. Ko, A. Luce, W. Fan, K. Liu, J. Zhou, Y.-S. Huang, C.-H. Ho, J. Yan, D. F. Ogletree, S. Aloni, J. Ji, S. Li, J. Li, F. M. Peeters, and J. Wu, *Nat. Commun.* **5**, 3252 (2014).
- [36] S. Yang, C. Wang, H. Sahin, H. Chen, Y. Li, S.-S. Li, A. Suslu, F. M. Peeters, Q. Liu, J. Li, and S. Tongay, *Nano Lett.* **15**, 1660 (2015).
- [37] D. A. Chenet, O. B. Aslan, P. Y. Huang, C. Fan, A. M. van der Zande, T. F. Heinz, and J. C. Hone, *Nano Lett.* **15**, 5667 (2015).
- [38] J. O. Island, M. Buscema, M. Barawi, J. M. Clamagirand, J. R. Ares, C. Sanchez, I. J. Ferrer, G. A. Steele, H. S. J. van der Zant, and A. Castellanos-Gomez, *Adv. Opt. Mater.* **2**, 641 (2014).
- [39] J. Dai and X. C. Zeng, *Angew. Chem.* **127**, 7682 (2015).
- [40] J. Kang, H. Sahin, H. D. Ozaydin, R. T. Senger, and F. M. Peeters, *Phys. Rev. B* **92**, 075413 (2015).